Supplementary Information (SI) for Molecular Systems Design & Engineering.

# Supporting Information: Quantum Chemical Screening of Eutectic Solvent Components for Insights into $CO_2$ Complexation Mechanisms

Stephen P. Vicchio,[*,†] Osasumwen Ikponmwosa,[‡] and Rachel B. Getman[*,‡]

[†]*Department of Chemical and Biomolecular Engineering, Clemson University, Clemson, SC 29634, United States*

[‡]*William G. Lowrie Department of Chemical and Biomolecular Engineering, Ohio State University, Columbus, OH 43210, United States*

E-mail: stephen.vicchio@uky.edu; getman.11@osu.edu

# Contents

# S1 General Structural Information

Table S1: The structure name, type, and abbreviation for the different $[\mathrm{HBAc}]^+$ species included in the structure library.

| Structure | Type | Abbreviation |
|---|---|---|
| Choline | $[\mathrm{HBAc}]^+$ | $[\mathrm{Ch}]^+$ |
| 1-Ethyl-3-methylimidazolium | $[\mathrm{HBAc}]^+$ | $[\mathrm{EMIM}]^+$ |
| 3-Ethylthiazolium | $[\mathrm{HBAc}]^+$ | $[\mathrm{ETH}]^+$ |
| 3-Ethyl-4,5-dimethylthiazolium | $[\mathrm{HBAc}]^+$ | $[\mathrm{EMMTH}]^+$ |
| 3-Ethyl-5-(hydroxymethyl)thiazolium | $[\mathrm{HBAc}]^+$ | $[\mathrm{EHMTH}]^+$ |

Table S2: The structure name, type, and abbreviation for the different $[\mathrm{HBAa}]^-$ species included in the structure library.

| Structure | Type | Abbreviation |
|---|---|---|
| Imidazolide | $[\mathrm{HBAa}]^-$ | $[\mathrm{Im}]^-$ |
| 2-Methylimidazolide | $[\mathrm{HBAa}]^-$ | $[\mathrm{MeIm}]^-$ |
| 2-Ethylimidazolide | $[\mathrm{HBAa}]^-$ | $[\mathrm{EtIm}]^-$ |
| Tetrazolide | $[\mathrm{HBAa}]^-$ | $[\mathrm{Tz}]^-$ |
| 2-Cyanopyrrolide | $[\mathrm{HBAa}]^-$ | $[2-\mathrm{CNpyr}]^-$ |
| Pyrazolide | $[\mathrm{HBAa}]^-$ | $[\mathrm{Pyz}]^-$ |
| Pyrrolide | $[\mathrm{HBAa}]^-$ | $[\mathrm{Pyr}]^-$ |
| 1,2,3-Triazolide | $[\mathrm{HBAa}]^-$ | $[123-\mathrm{Trz}]^-$ |
| 1,2,4-Triazolide | $[\mathrm{HBAa}]^-$ | $[124-\mathrm{Trz}]^-$ |
| Benzotriazolide | $[\mathrm{HBAa}]^-$ | $[\mathrm{B}-\mathrm{Trz}]^-$ |
| Indazolide | $[\mathrm{HBAa}]^-$ | $[\mathrm{Ind}]^-$ |
| Benzimidazolide | $[\mathrm{HBAa}]^-$ | $[\mathrm{BIm}]^-$ |

Table S3: The structure name, type, and abbreviation for the different HBD species included in the structure library.

| Structure | Type | Abbreviation |
|---|---|---|
| 1,5-Pentanediamine | HBD | PDA |
| 1,3-Propanediamine | HBD | TDA |
| 1,2-Ethanediamine | HBD | EDA |
| Monoethanolamine | HBD | MEA |
| Ethylene Glycol | HBD | EG |
| Propylene Glycol | HBD | PG |
| Glycerol | HBD | GOL |

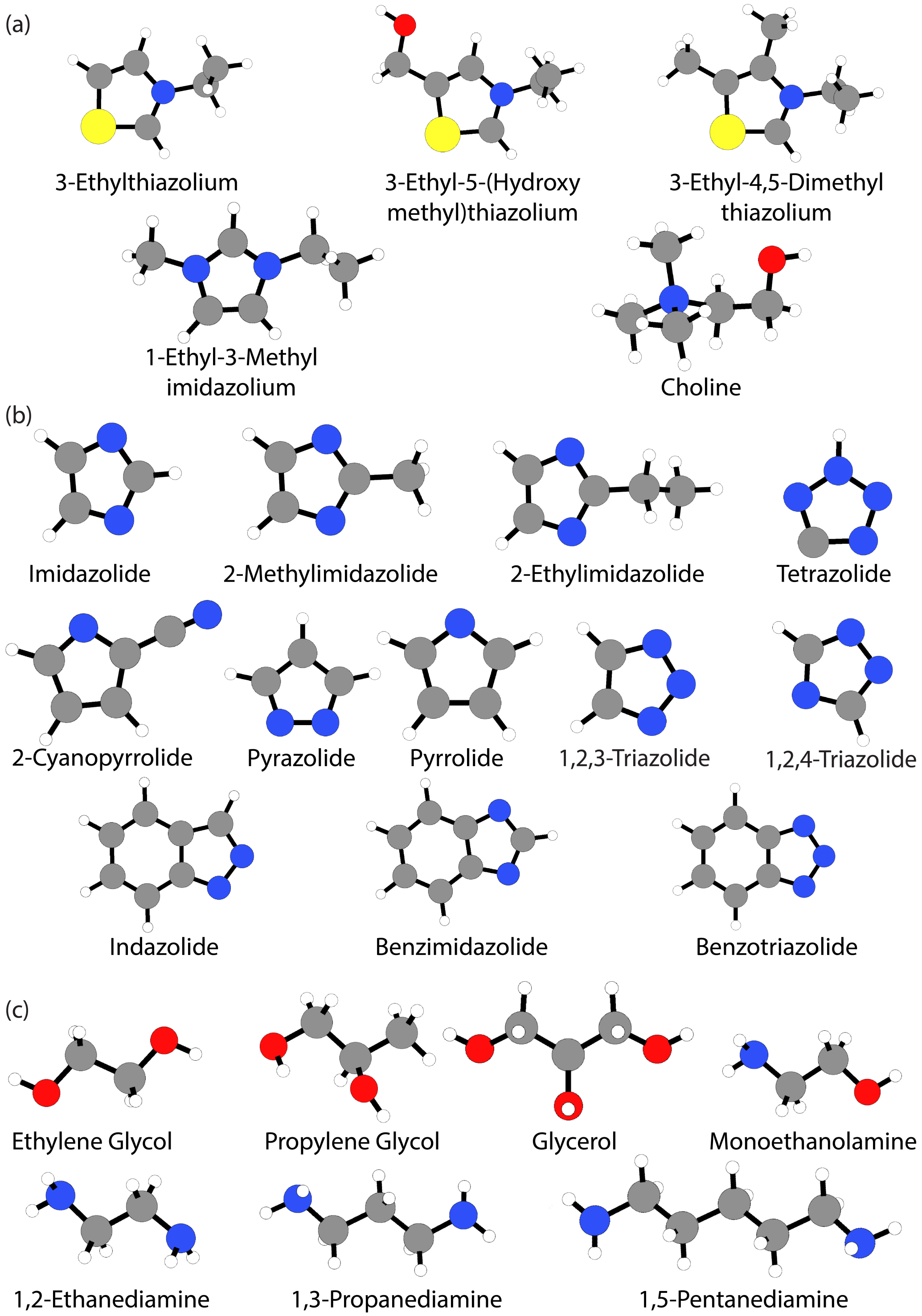

Figure S1: The (a) $[\mathrm{HBAc}]^{+}$, (b) $[\mathrm{HBAa}]^{-}$, and (c) HBD species included in the structure library. The structure served as the basis for all the hypothetical reactions associated with the different $CO_2$ complexation pathways, as discussed in Table 1 and Figure 3 of the main text. Atom color key: blue = nitrogen, red = oxygen, gray = carbon, yellow = sulfur, and white = hydrogen.

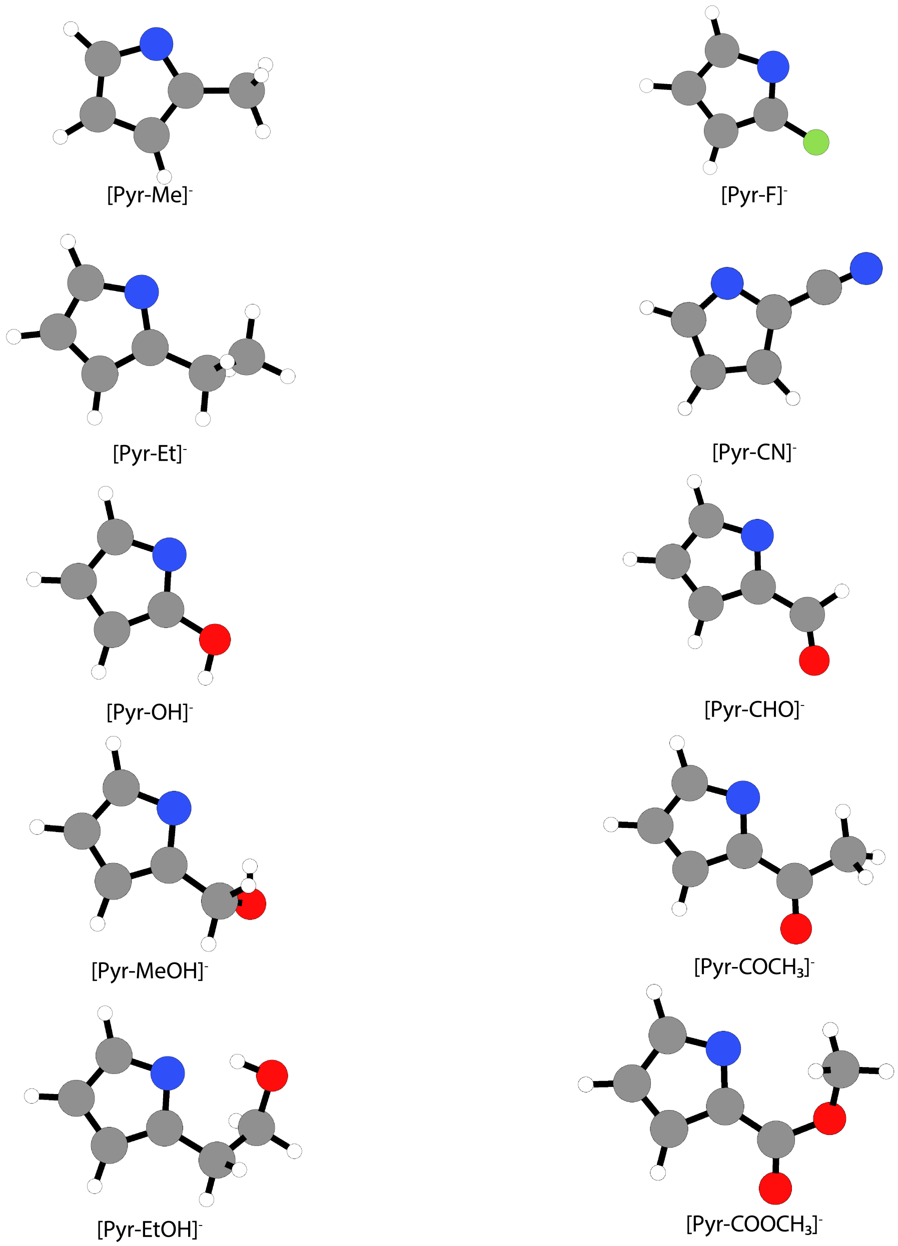

[Pyr-Me]$^-$

[Pyr-F]$^-$

[Pyr-Et]$^-$

[Pyr-CN]$^-$

[Pyr-OH]$^-$

[Pyr-CHO]$^-$

[Pyr-MeOH]$^-$

[Pyr-COCH$_3$]$^-$

[Pyr-EtOH]$^-$

[Pyr-COOCH$_3$]$^-$

Figure S2: The [Pyr$-$R]$^-$, ligand functionalized structures used to investigate the CO$_2$ binding reactions (Reaction **R2**) with different ligand environments. Atom color key: blue = nitrogen, red = oxygen, gray = carbon, yellow = sulfur, and white = hydrogen.

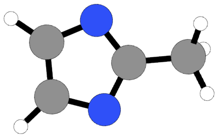

[Pyr-Me]$^-$

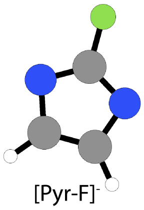

[Pyr-F]$^-$

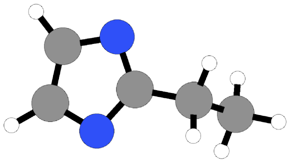

[Pyr-Et]$^-$

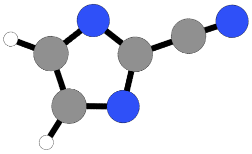

[Pyr-CN]$^-$

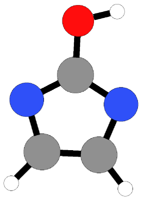

[Pyr-OH]$^-$

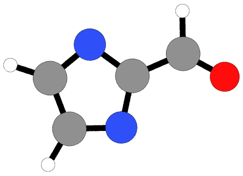

[Pyr-CHO]$^-$

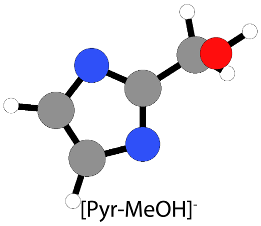

[Pyr-MeOH]$^-$

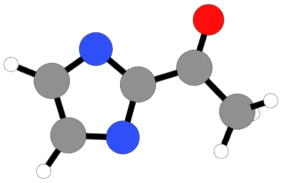

[Pyr-COCH$_3$]$^-$

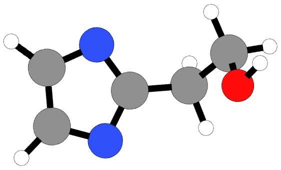

[Pyr-EtOH]$^-$

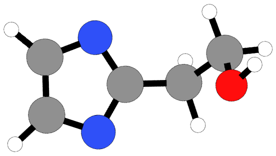

[Pyr-COOCH$_3$]$^-$

Figure S3: The [Im$-$R]$^-$, ligand functionalized structures used to investigate the $CO_2$ binding reactions (Reaction **R2**) with different ligand environments. Atom color key: blue = nitrogen, red = oxygen, gray = carbon, yellow = sulfur, and white = hydrogen.

# S2 Implicit Solvation Considerations

Klemm et al. uses implicit solvation to simulate the liquid structure (i.e., the hydrogen bonding network) of $[\mathrm{Ch}]^{+}[\mathrm{Pro}]^{-}$:EG eutectic solvent.[1] The high-throughput screening approach also requires implicitly capturing the liquid structure, as the hydrogen bond network stabilizes the ionic species present in the eutectic solvent. Now, the dielectric constant for ionic liquids and eutectic solvents is a function of species present (i.e., the $[\mathrm{HBAc}]^{+}$, $[\mathrm{HBAa}]^{-}$, and HBD). Given all the different combinations of structures considered during high-throughput screening, determining a dielectric constant for each unique combination wasn't feasible. In theory, each of the eutectic solvent (i.e., 420 $[\mathrm{HBAc}]^{+}[\mathrm{HBAa}]^{-}$:HBD combinations) requires a specific dielectric constant. Additionally, the specific dielectric constant would be a function of the molar ratio between the $[\mathrm{HBAc}]^{+}[\mathrm{HBAa}]^{-}$ and the HBD. Hence, a representative dielectric constant is needed.

A representative dielectric constant was selected using a series of test calculations on the $[\mathrm{HBAc}]^{+}$, $[\mathrm{HBAa}]^{-}$, and HBD pathways for the $[\mathrm{EMMTH}]^{+}[\mathrm{IMID}]^{-}$:MEA eutectic solvent. The influence of the dielectric constant on the calculated pathway energies are presented in Table S4. In G16, 'None ($\epsilon = 0.0000$)' represents the pathway energies from gas phase DFT calculations (i.e., no solvent is included). The dielectric constant was then systematically varied from 'None $\epsilon = 0.0000$' to 'Water $\epsilon = 78.3553$', with 'None' and 'Water' representing extreme cases of the dielectric constant values. The other dielectric constants include toluene ($\epsilon = 2.3741$), 1,2-dichloroethane ($\epsilon = 10.125$), and ethanol ($\epsilon = 24.8520$). The same analysis is performed with the inclusion of dispersion corrections (Table S5).

Table S4: Understanding the role of implicit solvation on the pathway free energies ($\Delta G^c$) in units of kJ/mol by varying the dielectric constant for the [EMMTH]$^+$[IMID]$^-$:MEA eutectic solvent.

| Pathway | None<br>$\epsilon = 0.0000$ | Toluene<br>$\epsilon = 2.3741$ | 1,2-Dichloroethane<br>$\epsilon = 10.125$ | Ethanol<br>$\epsilon = 24.8520$ | Water<br>$\epsilon = 78.3553$ |
|---|---|---|---|---|---|
| HBAc | -396.0 | -186.9 | -84.9 | -67.7 | -59.8 |
| [HBAa]$^-$ | -85.1 | -69.7 | -60.4 | -58.7 | -57.9 |
| [HBD]$^-$ | -43.1 | -45.0 | -54.7 | -57.3 | -58.6 |

Table S5: Understanding the role of implicit solvation on the pathway free energies ($\Delta G^c$) in units of kJ/mol by varying the dielectric constant for the [EMMTH]$^+$[IMID]$^-$:MEA eutectic solvent with dispersion corrections.

| Pathway | None<br>$\epsilon = 0.0000$ | 1,2-Dichloroethane<br>$\epsilon = 10.125$ | Ethanol<br>$\epsilon = 24.8520$ | Water<br>$\epsilon = 78.3553$ |
|---|---|---|---|---|
| HBAc | -416.4 | -105.1 | -87.9 | -80.0 |
| [HBAa]$^-$ | -99.6 | -75.1 | -73.4 | -72.5 |
| [HBD]$^-$ | -50.8 | -67.7 | -70.3 | -71.6 |

Significant differences in energies for the [HBAc]$^+$ pathway using gas phase energies are observed due to the lack of stabilization of the cationic species (Table S4). Without implicitly considering the liquid structure (i.e., no dielectric constant, $\epsilon = 0.0000$), the [HBAc]$^+$ pathway energies are significantly downhill (-396.0 kJ/mol).

By just including the liquid structure with a small dielectric constant (i.e., toluene ($\epsilon = 2.3741$)), the same [HBAc]$^+$ pathway energy is calculated to be -186.9 kJ/mol. As the dielectric constant increases, the [HBAc]$^+$ pathway continues to become more positive, again suggesting that the [HBAc]$^+$ is highly sensitive to the liquid structure. When inspecting the electronic energies for each structure, the energy of the cationic species ([HBAc]$^+$) drives the fluctuations in the [HBAc]$^+$ pathway energies. For both [HBAa]$^-$ and the HBD pathways, the difference in pathway energies is less sensitive to liquid structure. Increasing the dielectric constant from $\epsilon = 0.0000$ to $\epsilon = 78.3553$ increases the $[\text{HBAa}]^-$ pathway energies by 27.2 kJ/mol and decreases the HBD pathway energies by 15.5 kJ/mol. Therefore, including implicit solvation becomes necessary to capture the electronic structure correctly. In Table S5, the same analysis as Table S4 with the addition of dispersion corrections. A similar observation as the dielectric constant is observed when the dispersion corrections are included.

In summary, calculating representative electronic energies requires considering the liquid structure by selecting a dielectric constant. Ultimately, ethanol ($\epsilon = 24.8520$) is chosen to represent the solvation environment in the high-throughput DFT calculations. Only minor changes in the energies between ethanol ($\epsilon = 24.8520$) and water $\epsilon = 78.3553$ are observed, suggesting that the energies start to plateau when the dielectric constant increases. Dispersion corrections were also included in the DFT electronic energies.

# S3 Explicit $[\mathrm{HBAa}]^-$ Considerations

In the main text, Figure 4 shows the $CO_2$ complexation energies for the $[\mathrm{HBAa}]^-$ species. These figures only include implicit solvation to model the hydrogen bond network, which was needed to accurately model the electronic structure of the different species (as discussed in SI Section *2.0 Implicit Solvation Considerations*). Additional insights are provided by considering explicit HBD species for intermediates involved in Reaction **R2** (i.e., the $[\mathrm{HBAa}]^-$ complexation pathway). By explicitly considering the HBD, further complexity is introduced into the model and required additional DFT calculations. For example, each $[\mathrm{HBAa}]^-$ and $[\mathrm{HBAa{-}CO_2}]^-$ required inclusion of an HBD (Figure S4). The inclusion of explicit HBD is two-fold: (1) to validate the implicit modeling approach and (2) to understand how the hydrogen bond stabilization can impact the pathway energies.

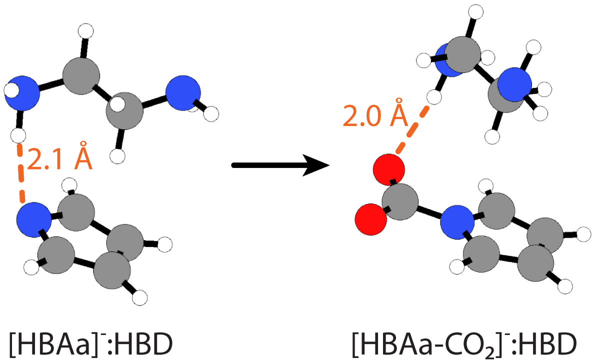

Figure S4: An example of explicit hydrogen bond stabilization for both $[\mathrm{HBAa}]^-$ and $[\mathrm{HBAa{-}CO_2}]^-$. The hydrogen bond is labeled in orange for both structures (with the distance also provided).

Similar trends for the $[\mathrm{HBAa}]^-$ complexation energies are observed between implicit solvation (Figure 4; main text) and explicit hydrogen bond stabilization (Figure S5a). Although the energies reported in Figure S5b fluctuate, $\Delta\Delta G$, generally, lead to a lowering ($\Delta\Delta G < 0$) of the $[\mathrm{HBA}]^-$ pathway energy. However, these values are below 25 kJ/mol, except for $[\mathrm{Tz}]^-$/EDA (−31.2 kJ/mol), $[\mathrm{Tz}]^-$/EG (−47.5 kJ/mol), and $[\mathrm{Tz}]^-$/GOL (−44.1 kJ/mol). Given the relative simplicity of our models (needed because any further complexity would prohibit high throughput screening), these errors are likely within the standard error of our simulations. The finding suggests that implicit solvation is a reasonable approximation for the purposes of high throughput screening. As with most endeavors into high throughput screening, promising systems should be checked with more sophisticated models if better accuracy in the calculated free energies is needed.

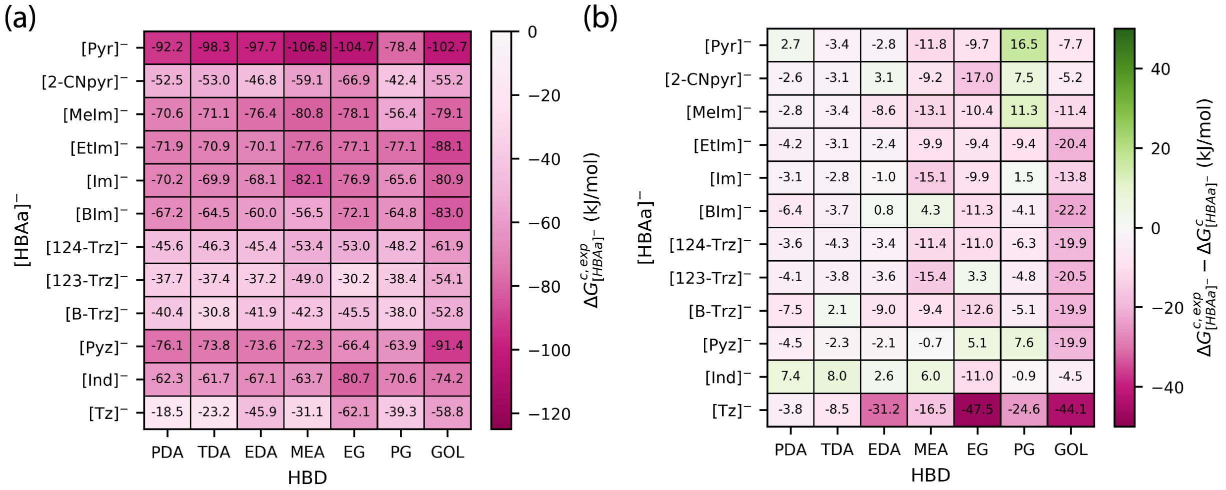

(a)

| $[HBAa]^-$ | PDA | TDA | EDA | MEA | EG | PG | GOL |
|---|---|---|---|---|---|---|---|
| $[Pyr]^-$ | -92.2 | -98.3 | -97.7 | -106.8 | -104.7 | -78.4 | -102.7 |
| $[2\text{-}CNpyr]^-$ | -52.5 | -53.0 | -46.8 | -59.1 | -66.9 | -42.4 | -55.2 |
| $[MeIm]^-$ | -70.6 | -71.1 | -76.4 | -80.8 | -78.1 | -56.4 | -79.1 |
| $[EtIm]^-$ | -71.9 | -70.9 | -70.1 | -77.6 | -77.1 | -77.1 | -88.1 |
| $[Im]^-$ | -70.2 | -69.9 | -68.1 | -82.1 | -76.9 | -65.6 | -80.9 |
| $[BIm]^-$ | -67.2 | -64.5 | -60.0 | -56.5 | -72.1 | -64.8 | -83.0 |
| $[124\text{-}Trz]^-$ | -45.6 | -46.3 | -45.4 | -53.4 | -53.0 | -48.2 | -61.9 |
| $[123\text{-}Trz]^-$ | -37.7 | -37.4 | -37.2 | -49.0 | -30.2 | -38.4 | -54.1 |
| $[B\text{-}Trz]^-$ | -40.4 | -30.8 | -41.9 | -42.3 | -45.5 | -38.0 | -52.8 |
| $[Pyz]^-$ | -76.1 | -73.8 | -73.6 | -72.3 | -66.4 | -63.9 | -91.4 |
| $[Ind]^-$ | -62.3 | -61.7 | -67.1 | -63.7 | -80.7 | -70.6 | -74.2 |
| $[Tz]^-$ | -18.5 | -23.2 | -45.9 | -31.1 | -62.1 | -39.3 | -58.8 |

(b)

| $[HBAa]^-$ | PDA | TDA | EDA | MEA | EG | PG | GOL |
|---|---|---|---|---|---|---|---|
| $[Pyr]^-$ | 2.7 | -3.4 | -2.8 | -11.8 | -9.7 | 16.5 | -7.7 |
| $[2\text{-}CNpyr]^-$ | -2.6 | -3.1 | 3.1 | -9.2 | -17.0 | 7.5 | -5.2 |
| $[MeIm]^-$ | -2.8 | -3.4 | -8.6 | -13.1 | -10.4 | 11.3 | -11.4 |
| $[EtIm]^-$ | -4.2 | -3.1 | -2.4 | -9.9 | -9.4 | -9.4 | -20.4 |
| $[Im]^-$ | -3.1 | -2.8 | -1.0 | -15.1 | -9.9 | 1.5 | -13.8 |
| $[BIm]^-$ | -6.4 | -3.7 | 0.8 | 4.3 | -11.3 | -4.1 | -22.2 |
| $[124\text{-}Trz]^-$ | -3.6 | -4.3 | -3.4 | -11.4 | -11.0 | -6.3 | -19.9 |
| $[123\text{-}Trz]^-$ | -4.1 | -3.8 | -3.6 | -15.4 | 3.3 | -4.8 | -20.5 |
| $[B\text{-}Trz]^-$ | -7.5 | 2.1 | -9.0 | -9.4 | -12.6 | -5.1 | -19.9 |
| $[Pyz]^-$ | -4.5 | -2.3 | -2.1 | -0.7 | 5.1 | 7.6 | -19.9 |
| $[Ind]^-$ | 7.4 | 8.0 | 2.6 | 6.0 | -11.0 | -0.9 | -4.5 |
| $[Tz]^-$ | -3.8 | -8.5 | -31.2 | -16.5 | -47.5 | -24.6 | -44.1 |

Figure S5: Heat maps showing (a) $[\text{HBAa}]^-$ $CO_2$ complexation pathway free energies ($\Delta G^{c,exp}_{[HBAa]^-}$) including hydrogen bond stabilization from the HBD species and (b) the difference between the explicit and implicit $CO_2$ complexation pathway free energies ($\Delta G^{c,exp}_{[HBAa]^-} - \Delta G^{c}_{[HBAa]^-}$). The values of $\Delta G^{c}_{[HBAa]^-}$ are the pathway free energies reported in Figure 4 (main text).

# S4 Additional Figures and Tables Referred to in the Main Text

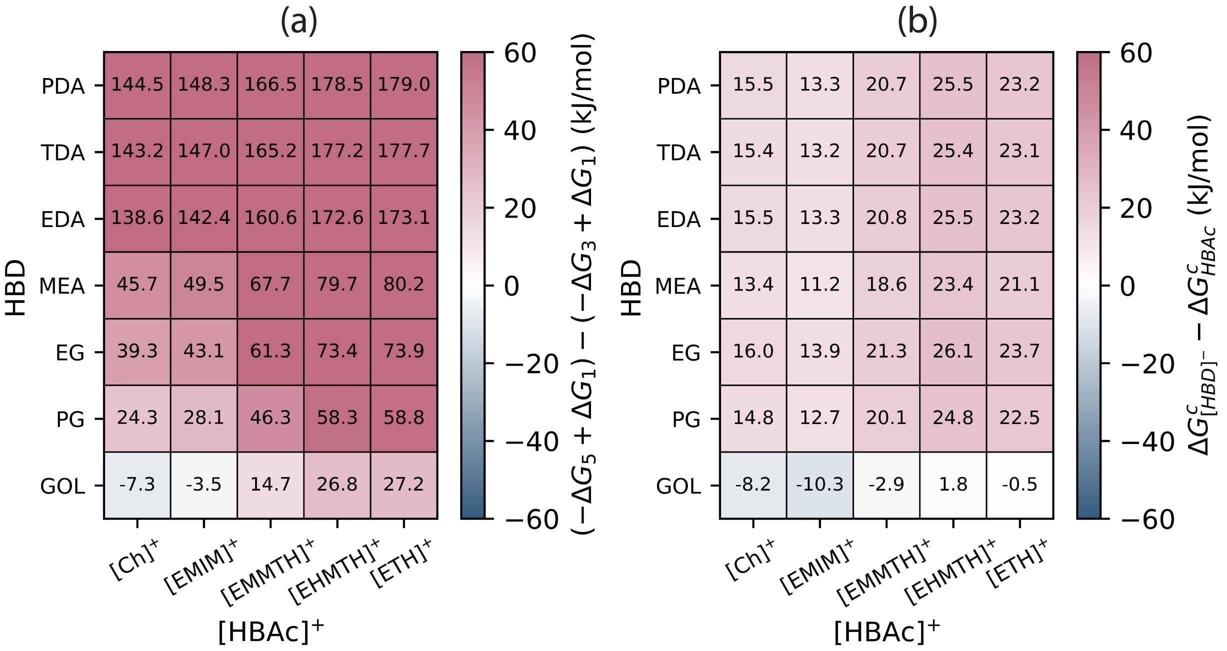

(a)

| HBD | [Ch]$^+$ | [EMIM]$^+$ | [EMMTH]$^+$ | [EHMTH]$^+$ | [ETH]$^+$ |
|---|---|---|---|---|---|
| PDA | 144.5 | 148.3 | 166.5 | 178.5 | 179.0 |
| TDA | 143.2 | 147.0 | 165.2 | 177.2 | 177.7 |
| EDA | 138.6 | 142.4 | 160.6 | 172.6 | 173.1 |
| MEA | 45.7 | 49.5 | 67.7 | 79.7 | 80.2 |
| EG | 39.3 | 43.1 | 61.3 | 73.4 | 73.9 |
| PG | 24.3 | 28.1 | 46.3 | 58.3 | 58.8 |
| GOL | -7.3 | -3.5 | 14.7 | 26.8 | 27.2 |

(b)

| HBD | [Ch]$^+$ | [EMIM]$^+$ | [EMMTH]$^+$ | [EHMTH]$^+$ | [ETH]$^+$ |
|---|---|---|---|---|---|
| PDA | 15.5 | 13.3 | 20.7 | 25.5 | 23.2 |
| TDA | 15.4 | 13.2 | 20.7 | 25.4 | 23.1 |
| EDA | 15.5 | 13.3 | 20.8 | 25.5 | 23.2 |
| MEA | 13.4 | 11.2 | 18.6 | 23.4 | 21.1 |
| EG | 16.0 | 13.9 | 21.3 | 26.1 | 23.7 |
| PG | 14.8 | 12.7 | 20.1 | 24.8 | 22.5 |
| GOL | -8.2 | -10.3 | -2.9 | 1.8 | -0.5 |

Figure S6: Heat maps comparing the free energies between the $[\mathrm{HBD}]^-$ and HBAc pathways: (a) difference between the $[\mathrm{HBD}]^-$ pathway proton transfer step (-**R5** + **R1**; $-\Delta G_5 + \Delta G_1$) and the HBAc pathway proton transfer step (-**R3** + **R1**; $-\Delta G_3 + \Delta G_1$) and (b) difference between HBD ($\Delta G^c_{[HBD]^-}$) and HBAc ($\Delta G^c_{[HBAa]^+}$) complexation pathways. The expressions for the different pathways are presented in Figure 3 of the main text. For the proton transfer steps, the energy ($\Delta G_1$) is calculated using $[\mathrm{Im}]^-$ as the proton acceptor. Swapping out the different $[\mathrm{HBAa}]^-$ species would only shift all energies, accordingly. The color bar indicates the more favorable pathway. For (a), blue indicates $[\mathrm{HBD}]^-$ proton transfer is more favorable ($-\Delta G_5 + \Delta G_1 < -\Delta G_3 + \Delta G_1$) and mauve indicates the $[\mathrm{HBAc}]^+$ proton transfer is more favorable ($-\Delta G_5 + \Delta G_1 > -\Delta G_3 + \Delta G_1$). For (b), blue indicates that the HBD complexation is preferred ($\Delta G^c_{[HBD]^-} < \Delta G^c_{HBAc}$) and mauve indicates that the HBAc complexation pathway is preferred ($\Delta G^c_{[HBD]^-} > \Delta G^c_{HBAc}$).

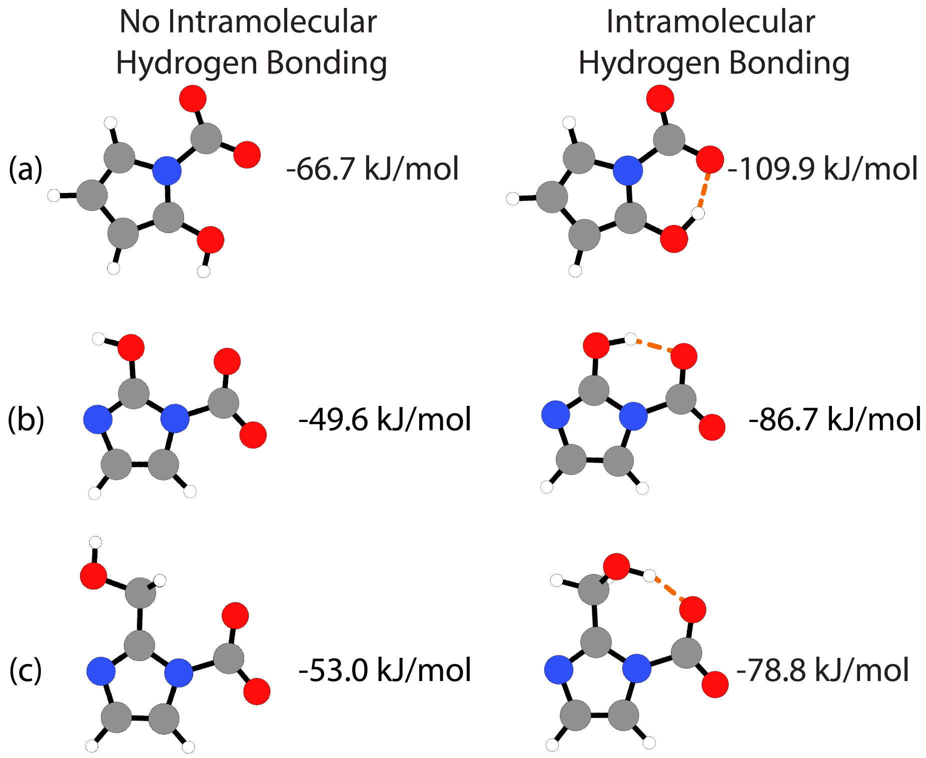

Figure S7: Structures (a) [Pyr−MeOH]$^-$, (b) [Im−MeOH]$^-$, and (c) [Im−EtOH]$^-$ illustrating hydrogen bond stabilization due to the inclusion of the R−OH groups at *ortho*-positions relative to the N atom $CO_2$ binding site. The $CO_2$ binding energy (**R2**; $\Delta G_2 = \Delta G^c$) for each structure is reported without (left column) and with (right column) intramolecular hydrogen bonding. The intramolecular hydrogen bonds are dashed, orange lines between the proton in OH and the complexed $CO_2$. Atom Color Key: Gray = Carbon, Blue = Nitrogen, Red = Oxygen, White = Oxygen.

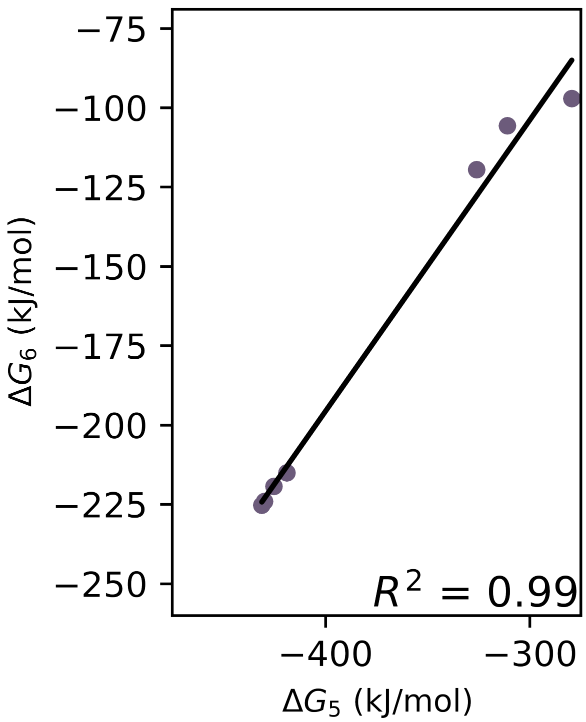

Figure S8: Scaling plots for the HBD species using the reaction free energies presented in Table 1 (main text). The proton transfer ($\Delta G_5$) and $CO_2$ binding ($\Delta G_6$) reactions are considered.

Table S6: Comparing Complexation Energies ($\boldsymbol{\Delta E^c}$) and Free Energies ($\boldsymbol{\Delta G^c}$) for the $[HBAa]^-$ Species at the b3lyp/6-311+G(d,p) (manuscript) and wB97XD/6-311+G(d,p) levels of theory. All energies are reported in kJ/mol

| | $\boldsymbol{\Delta E^c_{b3lyp}}$ | $\boldsymbol{\Delta E^c_{wB97XD}}$ | $\boldsymbol{\Delta G^c_{b3lyp}}$ | $\boldsymbol{\Delta G^c_{wB97XD}}$ |
|---|---|---|---|---|
| $[Pyr]^-$ | -103.2 | -105.8 | -94.9 | -97.0 |
| $[2-CNpyr]^-$ | -55.4 | -56.0 | -49.9 | -50.0 |
| $[MeIM]^-$ | -75.9 | -77.6 | -67.7 | -68.5 |
| $[EtIm]^-$ | -75.0 | -76.7 | -67.7 | -68.3 |
| $[Im]^-$ | -73.4 | -75.6 | -67.1 | -68.8 |
| $[BIm]^-$ | -64.4 | -66.5 | -60.8 | -62.3 |
| $[124-Trz]^-$ | -48.0 | -51.0 | -42.0 | -44.3 |
| $[123-Trz]^-$ | -38.6 | -41.2 | -33.6 | -35.6 |
| $[B-Trz]^-$ | -35.5 | -37.5 | -32.9 | -34.5 |
| $[Pyr]^-$ | -78.3 | -81.4 | -71.5 | -74.2 |
| $[Ind]^-$ | -74.7 | -78.2 | -69.7 | -73.0 |
| $[Tz]^-$ | -19.3 | -21.5 | -14.7 | -15.8 |

# S5 Trends between $CO_2$ Binding and Proton Transfer Free Energies

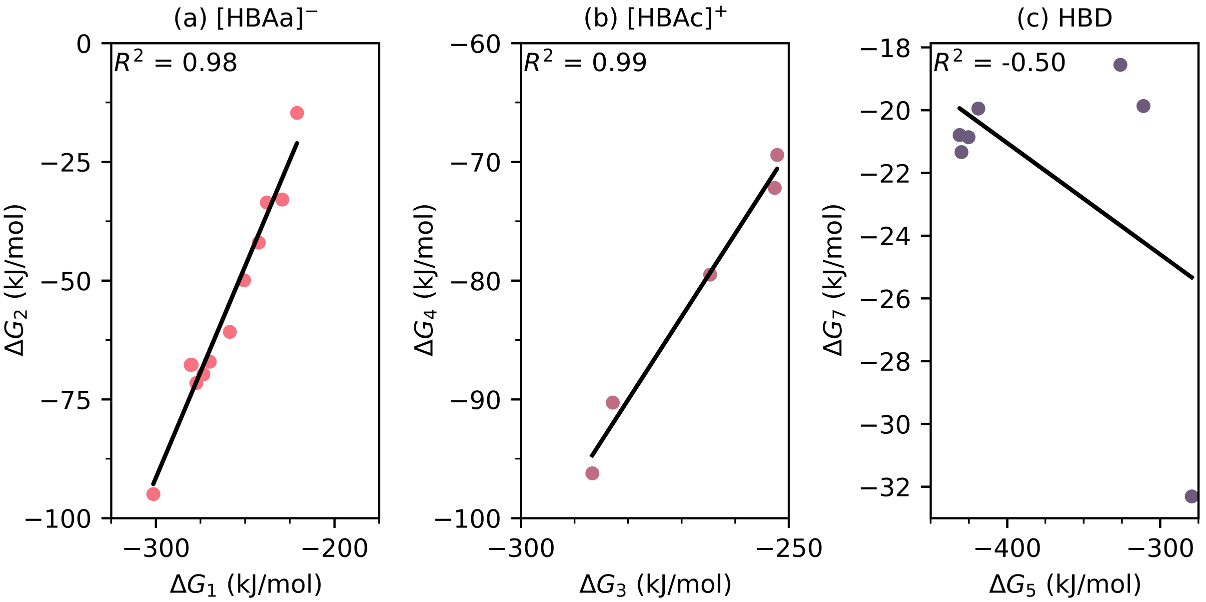

Figure S9: Scaling plots for the (a) $[HBAa]^-$, (b) $[HBAc]^+$, and (c) HBD species using the reaction free energies presented in Table 1 (main text). For (a), the proton transfer ($\Delta G_1$) and $CO_2$ binding ($\Delta G_2$) reactions are considered. For (b), the proton transfer ($\Delta G_3$) and $CO_2$ binding ($\Delta G_4$) reactions are considered. For (c), the proton transfer ($\Delta G_5$) and the weak $CO_2$ complexation ($\Delta G_7$) are considered.

The interplay between the $CO_2$ binding and proton transfer steps is fundamental to the $CO_2$ complexation process. Figure S9 explores the relationship between these species to identify the relationships between the different reaction steps. For the $[HBAa]^-$ species (Figure S9a), the more negative (i.e., stronger) the proton transfer free energy indicates a more negative (i.e., stronger) $CO_2$ binding energy that is attributed to the increased nucleophilicity of the $[HBAa]^-$. As discussed by Rheinhardt et al., most $CO_2$ sorption materials rely on nucleophiles to capture $CO_2$.[2] Nucleophiles contain electron lone pairs capable of forming chemical bonds. A $[HBAa]^-$ that strongly binds $CO_2$ is also likely to accept a proton from an $[HBAc]^+$ and/or HBD. When considering proton transfers, strong nucleophiles also utilize the electron-rich character to bind protons. These findings support the idea that there is a competitive process between $CO_2$ binding and proton affinity for an $[HBAa]^-$ species.

The same trend is observed for both $[HBAc]^+$ (Figure S9b) and $[HBD]^-$ species (Figure S8), i.e., a more negative proton transfer energy indicates a more negative $CO_2$ binding energy. Since the HBAc and $[HBD]^-$ rely on intermolecular proton transfers for $CO_2$ complexation, a stronger (more negative) proton transfer energy leads to unfavorable $CO_2$ binding thermodynamics. An $[HBAc]^+$ and/or $[HBD]^-$ species with a more negative proton transfer energy suggests that the species is less likely to donate a proton for $CO_2$ complexation.

The findings support the importance of intermolecular proton transfers in identifying $CO_2$ complexation in a given DESs/ESs, and suggest that descriptors such as proton affinity or pKa[3] could be useful when identifying candidate HBAc, $[HBAa]^-$, and $[HBD]^-$ species and/or predicting potential product distributions.

That said, as discussed above, HBD species can complex $CO_2$ via multiple pathways. We find that the pathway where $CO_2$ weakly complexes to the HBD prior to proton transfer is thermodynamically more likely to occur. By weakly complexating $CO_2$, the proton transfer to a $[HBAa]^-$ species becomes more favorable. Figure S9c compares this proton transfer ($\Delta G_5$) free energy with the free energy of weak $CO_2$ complexation ($\Delta G_7$). Unlike the results presented for the $[HBAa]^-$ and $[HBAc]^+$ species, there is not a strong correlation between these two free energies.

# S6 Raw Electronic Energies

Table S7: The electronic energies ($\boldsymbol{E}$), and the vibrational free energy correction terms at 1 atm and 25 °C ($\boldsymbol{G_{Vib}}$) for the $[\text{HBAc}]^+$ species (**Structure**). All raw electronic energies are presented in hartrees. The energies are organized by their the intermediate **Type** (i.e., Isolated, $CO_2$ binding, and Proton Transfer), with the **Chemical Naming** indicating the shorthand notation. The bracketed species (i.e., [ ]) are positively charged.

| **Structure** | **Type** | $\boldsymbol{E}$ | $\boldsymbol{E_{Vib}}$ **(hartree)** | $\boldsymbol{G_{Vib}}$ **(hartree)** |
|---|---|---|---|---|
| $[\text{EMMTH}]^+$ | Isolated | -726.910185 | 0.181712 | 0.167637 |
| $\text{EMMTH}-CO_2$ | $CO_2$ Binding | -915.106474 | 0.185957 | 0.165529 |
| EMMTH | Proton Transfer | -726.424136 | 0.168714 | 0.155064 |
| $[\text{EHMTH}]^+$ | Isolated | -762.811520 | 0.159261 | 0.145591 |
| $\text{EHMTH}-CO_2$ | $CO_2$ Binding | -951.009230 | 0.163378 | 0.143098 |
| EHMTH | Proton Transfer | -762.329564 | 0.146149 | 0.132525 |
| $[\text{ETH}]^+$ | Isolated | -648.236194 | 0.124680 | 0.117020 |
| $\text{ETH}-CO_2$ | $CO_2$ Binding | -836.433898 | 0.128832 | 0.115399 |
| ETH | Proton Transfer | -647.754754 | 0.111581 | 0.104290 |
| $[\text{Ch}]^+$ | Isolated | -328.896476 | 0.196997 | 0.186091 |
| $\text{Ch}-CO_2$ | $CO_2$ Binding | -517.092875 | 0.201280 | 0.186097 |
| Ch | Proton Transfer | -328.401478 | 0.182394 | 0.172951 |
| $[\text{EMIM}]^+$ | Isolated | -344.737992 | 0.168950 | 0.158392 |
| $\text{EMIM}-CO_2$ | $CO_2$ Binding | -532.931868 | 0.173012 | 0.156697 |
| EMIM | Proton Transfer | -344.243823 | 0.155186 | 0.144630 |

Table S8: The electronic energies ($\boldsymbol{E}$), and the vibrational free energy correct terms at 1 atm and 25 °C ($\boldsymbol{G_{Vib}}$) for the [HBAa]$^-$ species (**Structure**). All raw electronic energies are presented in hartrees. The energies are organized by their the intermediate **Type** (i.e., isolated, CO$_2$ binding, and Proton Transfer), with the **Chemical Naming** indicating the shorthand notation. The bracketed species (i.e., [ ]) are negatively charged.

| **Structure** | **Type** | $\boldsymbol{E}$ | $\boldsymbol{E_{Vib}}$ **(hartree)** | $\boldsymbol{G_{Vib}}$ **(hartree)** |
|---|---|---|---|---|
| [123−Trz]$^-$ | Isolated | -241.840863 | 0.044679 | 0.043871 |
| [123−Trz−CO$_2$]$^-$ | CO$_2$ Binding | -430.506855 | 0.061733 | 0.055481 |
| 123−Trz | Proton Transfer | -242.317712 | 0.058436 | 0.057427 |
| [124−Trz]$^-$ | Isolated | -241.863102 | 0.045257 | 0.044505 |
| [124−Trz−CO$_2$]$^-$ | CO$_2$ Binding | -430.532680 | 0.062206 | 0.056491 |
| 124−Trz | Proton Transfer | -242.341241 | 0.058627 | 0.057646 |
| [2−CNpyr]$^-$ | Isolated | -302.046811 | 0.067976 | 0.063868 |
| [2−CNpyr−CO$_2$]$^-$ | CO$_2$ Binding | -490.719186 | 0.085220 | 0.075630 |
| 2−CNpyr | Proton Transfer | -302.528102 | 0.081511 | 0.077011 |
| [EtIm]$^-$ | Isolated | -304.477871 | 0.113394 | 0.106516 |
| [EtIm−CO$_2$]$^-$ | CO$_2$ Binding | -493.157734 | 0.130802 | 0.118989 |
| EtIm | Proton Transfer | -304.970451 | 0.126986 | 0.119805 |
| [MeIm]$^-$ | Isolated | -265.149319 | 0.084478 | 0.079804 |
| [MeIm−CO$_2$]$^-$ | CO$_2$ Binding | -453.829523 | 0.101810 | 0.092611 |
| MeIm | Proton Transfer | -265.641803 | 0.097916 | 0.092787 |
| [B−Trz]$^-$ | Isolated | -395.535897 | 0.092351 | 0.087885 |
| [B−Trz−CO$_2$]$^-$ | CO$_2$ Binding | -584.200722 | 0.109264 | 0.098578 |
| B−Trz | Proton Transfer | -396.008826 | 0.105617 | 0.100831 |
| [BIm]$^-$ | Isolated | -379.522029 | 0.104290 | 0.099737 |
| [BIm−CO$_2$]$^-$ | CO$_2$ Binding | -568.197846 | 0.121478 | 0.110809 |
| BIm | Proton Transfer | -380.006097 | 0.117581 | 0.112624 |
| [Im]$^-$ | Isolated | -225.816524 | 0.056432 | 0.055463 |
| [Im−CO$_2$]$^-$ | CO$_2$ Binding | -414.495762 | 0.073552 | 0.067557 |
| Im | Proton Transfer | -226.305004 | 0.069757 | 0.068513 |
| [Ind]$^-$ | Isolated | -379.490058 | 0.103758 | 0.099042 |
| [Ind−CO$_2$]$^-$ | CO$_2$ Binding | -568.169792 | 0.121228 | 0.110631 |
| Ind | Proton Transfer | -379.980146 | 0.117474 | 0.112342 |
| [Pyz]$^-$ | Isolated | -225.793753 | 0.055934 | 0.054910 |
| [Pyz−CO$_2$]$^-$ | CO$_2$ Binding | -414.474860 | 0.073303 | 0.067166 |
| Pyz | Proton Transfer | -226.285601 | 0.069717 | 0.068466 |
| [Pyr]$^-$ | Isolated | -209.748912 | 0.067022 | 0.065760 |
| [Pyr−CO$_2$]$^-$ | CO$_2$ Binding | -398.439527 | 0.084653 | 0.078614 |
| Pyr | Proton Transfer | -210.249814 | 0.080740 | 0.079178 |
| [Tz]$^-$ | Isolated | -257.818326 | 0.033038 | 0.032194 |
| [Tz−CO$_2$]$^-$ | CO$_2$ Binding | -446.476978 | 0.049808 | 0.043660 |
| Tz | Proton Transfer | -258.288767 | 0.046663 | 0.045805 |

Table S9: The electronic energies ($\boldsymbol{E}$), and the vibrational free energy correct terms at 1 atm and 25 °C ($\boldsymbol{G_{Vib}}$) for the HBD species (**Structure**). All raw electronic energies are presented in hartrees. The energies are organized by their the intermediate **Type** (i.e., isolated, $CO_2$ binding, Proton Transfer, and Weak $CO_2$ Binding), with the **Chemical Naming** indicating the shorthand notation. The bracketed species (i.e., $[]^-$) are negatively charged.

| **Structure** | **Type** | $\boldsymbol{E}$ | $\boldsymbol{E_{Vib}}$ **(hartree)** | $\boldsymbol{G_{Vib}}$ **(hartree)** |
|---|---|---|---|---|
| EDA | Isolated | -190.606500 | 0.109563 | 0.104841 |
| $[EDA-CO_2]^-$ | $CO_2$ Binding | -378.796833 | 0.113913 | 0.104681 |
| $[EDA]^-$ | Proton Transfer | -190.056825 | 0.094207 | 0.089814 |
| $EDA-CO_2$ | Weak $CO_2$ Binding | -379.262278 | 0.125802 | 0.111076 |
| EG | Isolated | -230.349123 | 0.084494 | 0.079266 |
| $[EG-CO_2]^-$ | $CO_2$ Binding | -418.540312 | 0.088998 | 0.080175 |
| $[EG]^-$ | Proton Transfer | -229.839282 | 0.070281 | 0.066264 |
| $EG-CO_2$ | Weak $CO_2$ Binding | -419.004219 | 0.100842 | 0.085696 |
| GLY | Isolated | -344.925361 | 0.118632 | 0.108581 |
| $[GLY-CO_2]^-$ | $CO_2$ Binding | -533.127594 | 0.123297 | 0.111305 |
| $[GLY]^-$ | Proton Transfer | -344.436382 | 0.105158 | 0.098686 |
| $GLY-CO_2$ | Weak $CO_2$ Binding | -533.586957 | 0.135279 | 0.116270 |
| MEA | Isolated | -210.477898 | 0.097036 | 0.092099 |
| $[MEA-CO_2]^-$ | $CO_2$ Binding | -398.667470 | 0.101379 | 0.092049 |
| $[MEA]^-$ | Proton Transfer | -209.965626 | 0.082777 | 0.079085 |
| $MEA-CO_2$ | Weak $CO_2$ Binding | -399.132977 | 0.113389 | 0.098361 |
| $[MEA-CO_2]^-$ | $CO_2$ Binding | -398.668521 | 0.101326 | 0.091426 |
| $[MEA]^-$ | Proton Transfer | -209.930952 | 0.081801 | 0.077366 |
| $MEA-CO_2$ | Weak $CO_2$ Binding | -399.134000 | 0.113450 | 0.099006 |
| PDA | Isolated | -308.593507 | 0.195893 | 0.182516 |
| $[PDA-CO_2]^-$ | $CO_2$ Binding | -496.783343 | 0.200296 | 0.181845 |
| $[PDA]^-$ | Proton Transfer | -308.041340 | 0.180320 | 0.167229 |
| PDA | Weak $CO_2$ Binding | -497.249539 | 0.212174 | 0.189030 |
| PG | Isolated | -269.687774 | 0.112796 | 0.106483 |
| $[PG-CO_2]^-$ | $CO_2$ Binding | -457.878155 | 0.117092 | 0.106122 |
| $[PG]^-$ | Proton Transfer | -269.183850 | 0.098431 | 0.093665 |
| $PG-CO_2$ | Weak $CO_2$ Binding | -458.342906 | 0.129112 | 0.112448 |
| TDA | Isolated | -229.935024 | 0.138387 | 0.130945 |
| $[TDA-CO_2]^-$ | $CO_2$ Binding | -418.124852 | 0.142694 | 0.130244 |
| $[TDA]^-$ | Proton Transfer | -229.383408 | 0.122899 | 0.115723 |
| $TDA-CO_2$ | Weak $CO_2$ Binding | -418.590982 | 0.154605 | 0.137177 |

Table S10: The electronic energies (***E***), and the vibrational free energy correct terms at 1 atm and 25 °C ($G_{Vib}$) for the [HBAa]$^-$ species. All raw electronic energies are presented in hartrees. The energies are organized by their reaction **Type** (i.e., Isolated, $CO_2$ binding, and proton affinity), with the **Chemical Naming** indicating the shorthand notation. The bracketed species (i.e., [ ]) are negatively charged.

| **Structure** | **Type** | ***E*** | $E_{Vib}$ **(hartree)** | $G_{Vib}$ **(hartree)** |
|---|---|---|---|---|
| [Pyr−OH]$^-$ | Isolated | -285.000782 | 0.072256 | 0.068626 |
| [Pyr−OH−$CO_2$]$^-$ | $CO_2$ Binding | -473.697831 | 0.089467 | 0.082215 |
| [Pyr−MeOH]$^-$ | Isolated | -324.329962 | 0.101452 | 0.094805 |
| [Pyr−MeOH−$CO_2$]$^-$ | $CO_2$ Binding | -513.023030 | 0.119372 | 0.109273 |
| [Pyr−Me]$^-$ | Isolated | -249.080140 | 0.095063 | 0.090544 |
| [Pyr−Me−$CO_2$]$^-$ | $CO_2$ Binding | -437.769628 | 0.112910 | 0.103647 |
| [Pyr−Et]$^-$ | Isolated | -288.408662 | 0.123872 | 0.116674 |
| [Pyr−Et−$CO_2$]$^-$ | $CO_2$ Binding | -477.097852 | 0.141800 | 0.129918 |
| [Pyr−EtOH]$^-$ | Isolated | -363.665015 | 0.130151 | 0.122348 |
| [Pyr−EtOH−$CO_2$]$^-$ | $CO_2$ Binding | -552.351586 | 0.148023 | 0.135213 |
| [Pyr−CN]$^-$ | Isolated | -302.046811 | 0.067976 | 0.063868 |
| [Pyr−CN−$CO_2$]$^-$ | $CO_2$ Binding | -490.719186 | 0.085220 | 0.075630 |
| [Pyr−$COOCH_3$]$^-$ | Isolated | -437.718417 | 0.112698 | 0.102569 |
| [Pyr−$COOCH_3$−$CO_2$]$^-$ | $CO_2$ Binding | -626.391486 | 0.130242 | 0.115078 |
| [Pyr−F]$^-$ | Isolated | -309.025170 | 0.060124 | 0.057666 |
| [Pyr−F−$CO_2$]$^-$ | $CO_2$ Binding | -497.697575 | 0.077464 | 0.069553 |
| [Pyr−CHO]$^-$ | Isolated | -323.139326 | 0.078432 | 0.074046 |
| [Pyr−CHO−$CO_2$]$^-$ | $CO_2$ Binding | -511.810177 | 0.095785 | 0.085384 |
| [Pyr−$COCH_3$]$^-$ | Isolated | -362.474725 | 0.106798 | 0.098441 |
| [Pyr−$COCH_3$−$CO_2$]$^-$ | $CO_2$ Binding | -551.142874 | 0.124056 | 0.110560 |

Table S11: The electronic energies (**$E$**), and the vibrational free energy correct terms at 1 atm and 25 °C (**$G_{Vib}$**) for the $[HBAa]^-$ species. All raw electronic energies are presented in hartrees. The energies are organized by their reaction **Type** (i.e., Isolated, $CO_2$ binding, and proton affinity), with the **Chemical Naming** indicating the shorthand notation. The bracketed species (i.e., [ ]) are negatively charged.

| **Structure** | **Type** | **$E$** | **$E_{Vib}$ (hartree)** | **$G_{Vib}$ (hartree)** |
|---|---|---|---|---|
| $[Im{-}OH]^-$ | Isolated | -301.073811 | 0.061826 | 0.059090 |
| $[Im{-}OH{-}CO_2]^-$ | $CO_2$ Binding | -489.761000 | 0.078539 | 0.071668 |
| $[Im{-}EtOH]^-$ | Isolated | -379.722483 | 0.119375 | 0.110162 |
| $[Im{-}EtOH{-}CO_2]^-$ | $CO_2$ Binding | -568.410361 | 0.137007 | 0.124419 |
| $[Im{-}MeOH]^-$ | Isolated | -340.394265 | 0.090651 | 0.084316 |
| $[Im{-}MeOH{-}CO_2]^-$ | $CO_2$ Binding | -529.080004 | 0.108282 | 0.098457 |
| $[Im{-}Me]^-$ | Isolated | -265.149319 | 0.084478 | 0.079804 |
| $[Im{-}Me{-}CO_2]^-$ | $CO_2$ Binding | -453.829523 | 0.101810 | 0.092611 |
| $[Im{-}Et]^-$ | Isolated | -304.477871 | 0.113394 | 0.106516 |
| $[Im{-}Et{-}CO_2]^-$ | $CO_2$ Binding | -493.157734 | 0.130802 | 0.118989 |
| $[Im{-}F]^-$ | Isolated | -325.094445 | 0.049510 | 0.047471 |
| $[Im{-}F{-}CO_2]^-$ | $CO_2$ Binding | -513.758991 | 0.066459 | 0.058569 |
| $[Im{-}CN]^-$ | Isolated | -318.106245 | 0.056992 | 0.053209 |
| $[Im{-}CN{-}CO_2]^-$ | $CO_2$ Binding | -506.767929 | 0.073804 | 0.064179 |
| $[Im{-}CHO]^-$ | Isolated | -339.198605 | 0.067521 | 0.063501 |
| $[Im{-}CHO{-}CO_2]^-$ | $CO_2$ Binding | -527.859776 | 0.084436 | 0.074199 |
| $[Im{-}COOCH_3]^-$ | Isolated | -453.787050 | 0.102014 | 0.092594 |
| $[Im{-}COOCH_3{-}CO_2]^-$ | $CO_2$ Binding | -642.447806 | 0.119066 | 0.103463 |
| $[Im{-}COCH_3]^-$ | Isolated | -378.534525 | 0.095875 | 0.087802 |
| $[Im{-}COCH_3{-}CO_2]^-$ | $CO_2$ Binding | -567.194650 | 0.112572 | 0.098352 |

# S7 Reaction Energies

Table S12: The reaction free energies for the $[\text{HBAa}]^+$ species (in kJ/mol). $\Delta G_3$ represents the proton transfer free energy (Reaction **R3**), and $\Delta G_4$ represents the $CO_2$ binding free energy to the deprotonated $[\text{HBAa}]^+$ species (i.e., HBAa) according to Reaction **R4**. All free energies are reported at 1 atm and 25 °C.

| **Structure** | $\mathbf{\Delta G_3}$ | $\mathbf{\Delta G_4}$ |
|---|---|---|
| $[\text{EMMTH}]^+$ | -264.675445 | -79.485568 |
| $[\text{EHMTH}]^+$ | -252.637478 | -72.186786 |
| $[\text{ETH}]^+$ | -252.162454 | -69.407145 |
| $[\text{Ch}]^+$ | -286.683124 | -96.229789 |
| $[\text{EMIM}]^+$ | -282.871885 | -90.261736 |

Table S13: The reaction free energies for the $[\text{HBAa}]^-$ species (in kJ/mol). $\Delta G_1$ represents the proton transfer free energy (Reaction **R1**), and $\Delta G_2$ represents the $CO_2$ binding free energy (Reaction **R2**). All free energies are reported at 1 atm and 25 °C.

| **Structure** | $\mathbf{\Delta G_1}$ | $\mathbf{\Delta G_2}$ |
|---|---|---|
| $[123-\text{Trz}]^-$ | -237.937941 | -33.561692 |
| $[124-\text{Trz}]^-$ | -242.417260 | -41.990537 |
| $[2-\text{CNpyr}]^-$ | -250.688490 | -49.921740 |
| $[\text{EtIm}]^-$ | -279.942323 | -67.714724 |
| $[\text{MeIm}]^-$ | -280.496540 | -67.733830 |
| $[\text{B}-\text{Trz}]^-$ | -229.250550 | -32.905808 |
| $[\text{BIm}]^-$ | -258.650385 | -60.767646 |
| $[\text{Im}]^-$ | -269.808770 | -67.066982 |
| $[\text{Ind}]^-$ | -273.372075 | -69.697252 |
| $[\text{Pyz}]^-$ | -277.319822 | -71.546397 |
| $[\text{Pyr}]^-$ | -301.454040 | -94.943609 |
| $[\text{Tz}]^-$ | -220.970729 | -14.667836 |

Table S14: The reaction free energies for the HBD species (in kJ/mol). $\boldsymbol{\Delta G_5}$ represents the proton transfer free energy (Reaction **R5**); $\Delta G_6$ represents the $CO_2$ binding free energy to the deprotonated HBD (i.e., $[HBD]^-$) according to Reaction **R6**; $\Delta G_7$ represents $CO_2$ binding free energy of the weakly complexed $CO_2$ (Reaction **R6**); and $\Delta G_8$ represents the proton transfer free energy of the weakly complexed $CO_2$ intermediate (Reaction **R8**). All free energies are reported at 1 atm and 25 °C.

| **Structure** | $\boldsymbol{\Delta G_5}$ | $\boldsymbol{\Delta G_6}$ | $\boldsymbol{\Delta G_7}$ | $\boldsymbol{\Delta G_8}$ |
|---|---|---|---|---|
| EDA | -425.282589 | -219.339754 | -20.860085 | -226.802920 |
| EG | -326.014889 | -119.511675 | -18.556235 | -225.059449 |
| GLY | -279.401339 | -97.131186 | -32.313244 | -214.583397 |
| MEA | -332.366002 | -124.136404 | -18.951851 | -227.181449 |
| MEA | -418.889394 | -215.053754 | -19.945498 | -223.781138 |
| PDA | -431.142589 | -225.235955 | -20.790475 | -226.697110 |
| PG | -310.964094 | -105.673775 | -19.867368 | -225.157687 |
| TDA | -429.867846 | -224.018776 | -21.336188 | -227.185259 |

Table S15: The reaction free energies for the ligand functionalized $[Pyr{-}R]^-$ species (in kJ/-mol). $\boldsymbol{\Delta G_2}$ represents the $CO_2$ binding free energy (Reaction **R2**). All free energies are reported at 1 atm and 25 °C.

| **Structure** | $\boldsymbol{\Delta G_2}$ |
|---|---|
| $[Pyr{-}OH]^-$ | -109.9 |
| $[Pyr{-}MeOH]^-$ | -97.1 |
| $[Pyr{-}Me]^-$ | -91.3 |
| $[Pyr{-}Et]^-$ | -90.2 |
| $[Pyr{-}EtOH]^-$ | -84.3 |
| $[Pyr{-}CN]^-$ | -49.9 |
| $[Pyr{-}COOCH_3]^-$ | -49.8 |
| $[Pyr{-}F]^-$ | -49.7 |
| $[Pyr{-}CHO]^-$ | -47.0 |
| $[Pyr{-}COCH_3]^-$ | -37.9 |

Table S16: The reaction free energies for the ligand functionalized $[\mathrm{Im{-}R}]^-$ species (in kJ/-mol). $\boldsymbol{\Delta G_2}$ represents the $CO_2$ binding free energy (Reaction **R2**). All free energies are reported at 1 atm and 25 °C.

| **Structure** | $\boldsymbol{\Delta G_2}$ |
|---|---|
| $[\mathrm{Im{-}OH}]^-$ | -86.7 |
| $[\mathrm{Im{-}EtOH}]^-$ | -84.1 |
| $[\mathrm{Im{-}MeOH}]^-$ | -78.8 |
| $[\mathrm{Im{-}Me}]^-$ | -67.7 |
| $[\mathrm{Im{-}Et}]^-$ | -67.7 |
| $[\mathrm{Im{-}F}]^-$ | -31.1 |
| $[\mathrm{Im{-}CN}]^-$ | -23.9 |
| $[\mathrm{Im{-}CHO}]^-$ | -23.3 |
| $[\mathrm{Im{-}COOCH_3}]^-$ | -21.8 |
| $[\mathrm{Im{-}COCH_3}]^-$ | -20.9 |

# References

(1) Klemm, A.; Vicchio, S. P.; Bhattacharjee, S.; Cagli, E.; Park, Y.; Zeeshan, M.; Dikki, R.; Liu, H.; Kidder, M. K.; Getman, R. B.; Gurkan, B. Impact of Hydrogen Bonds on CO2 Binding in Eutectic Solvents: An Experimental and Computational Study toward Sorbent Design for CO2 Capture. ACS Sustainable Chemistry and Engineering **2023**, 11, 3740–3749.

(2) Rheinhardt, J. H.; Singh, P.; Tarakeshwar, P.; Buttry, D. A. Electrochemical capture and release of carbon dioxide. ACS Energy Letters **2017**, 2, 454–461.

(3) Bernhardsen, I. M.; Krokvik, I. R.; Perinu, C.; Pinto, D. D.; Jens, K. J.; Knuutila, H. K. Influence of pKa on solvent performance of MAPA promoted tertiary amines. International Journal of Greenhouse Gas Control **2018**, 68, 68–76.